

RESEARCH LETTER

10.1002/2015GL066145

Key Points:

- Contributions to tropical cyclone potential intensity trends are quantified
- Robust trends only in Atlantic, disagreement between data sources elsewhere
- TTL temperatures play a role in interannual variability of potential intensity

Supporting Information:

- Supporting Information S1

Correspondence to:

A. A. Wing,
awing@ldeo.columbia.edu

Citation:

Wing, A. A., K. Emanuel, and S. Solomon (2015), On the factors affecting trends and variability in tropical cyclone potential intensity, *Geophys. Res. Lett.*, *42*, 8669–8677, doi:10.1002/2015GL066145.

Received 9 SEP 2015

Accepted 24 SEP 2015

Accepted article online 1 OCT 2015

Published online 19 OCT 2015

On the factors affecting trends and variability in tropical cyclone potential intensity

Allison A. Wing^{1,2}, Kerry Emanuel¹, and Susan Solomon¹

¹Program in Atmospheres, Oceans, and Climate, Department of Earth, Atmospheric and Planetary Sciences, Massachusetts Institute of Technology, Cambridge, Massachusetts, USA, ²Lamont-Doherty Earth Observatory, Columbia University, Palisades, New York, USA

Abstract Tropical cyclone potential intensity (V_p) is controlled by thermodynamic air-sea disequilibrium and thermodynamic efficiency, which is a function of the sea surface temperature and the tropical cyclone's outflow temperature. Observed trends and variability in V_p in each ocean basin are decomposed into contributions from these two components. Robustly detectable trends are found only in the North Atlantic, where tropical tropopause layer (TTL) cooling contributes up to a third of the increase in V_p . The contribution from disequilibrium dominates the few statistically significant V_p trends in the other basins. The results are sensitive to the data set used and details of the V_p calculation, reflecting uncertainties in TTL temperature trends and the difficulty of estimating V_p and its components. We also find that 20–71% of the interannual variability in V_p is linked to the TTL, with correlations between detrended time series of thermodynamic efficiency and V_p occurring over all ocean basins.

1. Introduction

Understanding the cause of observed trends in tropical cyclone intensity and projecting how tropical cyclone activity will differ under climate change is a topic of great interest and importance. There is some evidence that tropical cyclone intensity has already changed, such as an increase in the power dissipation of North Atlantic tropical cyclones [Emanuel, 2005] and an increase in the intensities of the strongest tropical cyclones [Elsner *et al.*, 2008; Kossin *et al.*, 2013]. Future projections indicate that anthropogenic warming will cause the globally averaged intensity of tropical cyclones to increase, shifting toward stronger storms [Knutson *et al.*, 2010, and references therein]. Much of the previous work investigating the physical causes of these changes has focused on the sea surface temperature (either directly or indirectly), but several recent papers have addressed the role of upper atmosphere temperature changes in contributing to changes in tropical cyclone intensity [Emanuel *et al.*, 2013; Vecchi *et al.*, 2013; Ramsay, 2013; Kossin, 2014; Wang *et al.*, 2014].

Temperatures in the tropical tropopause layer and lower stratosphere exhibit both decadal trends and interannual variability. The lower stratosphere has cooled by ~ 0.5 K per decade since 1979 [Ramaswamy *et al.*, 2001; Randel *et al.*, 2009], which has been linked to ozone loss and the major volcanic eruptions of El Chichon and Mount Pinatubo that warmed the stratosphere in the early part of the record [Ramaswamy *et al.*, 2006; Thompson and Solomon, 2009]. Temperature trends in the tropical tropopause layer, however, are more uncertain [e.g., Randel and Wu, 2006; Fueglistaler *et al.*, 2009; Haimberger *et al.*, 2012]. The tropical tropopause layer (TTL) is a layer in the uppermost troposphere that also has some characteristics of the stratosphere, and in which temperatures are a result of a complex coupling between atmospheric dynamics, chemistry, and radiation. Atmospheric temperatures in the TTL may modulate tropical cyclone intensity, since the temperature of tropical cyclone outflow is approximately equivalent to the ambient tropopause temperature [Emanuel and Rotunno, 2011]. The outflow temperature is a key parameter in tropical cyclone potential intensity, which is the theoretical maximum intensity of a steady state tropical cyclone given the sea surface temperature and environmental profile of atmospheric temperature and humidity [Emanuel, 1986].

There is evidence that tropical cyclones are affected by TTL temperature in observations, global models, and idealized models. Emanuel *et al.* [2013] found that downward trends in tropical cyclone outflow temperature associated with TTL cooling contributed significantly to upward trends in potential intensity in the North Atlantic in radiosonde data and reanalyses. In this and other studies [Vecchi *et al.*, 2013; Kossin, 2014], the National Centers for Environmental Prediction (NCEP)/National Center for Atmospheric Research (NCAR)

reanalysis was found to overestimate the TTL cooling (and therefore the increase in potential intensity). In simulations with a high-resolution global model, *Vecchi et al.* [2013] found that cooling in the lower TTL increased potential intensity and increased the fraction of tropical cyclones that reach hurricane intensity. Further, *Ramsay* [2013] and *Wang et al.* [2014] performed idealized simulations of tropical cyclones in a state of radiative-convective equilibrium with an axisymmetric, nonhydrostatic model and a three-dimensional mesoscale model, respectively. In these studies, the potential intensity and modeled storm intensity increased at a rate of $0.4\text{--}1\text{ m s}^{-1}$ per degree of tropopause cooling. Sea surface warming resulted in a potential intensity trend of about 2 m s^{-1} per degree of warming [*Ramsay*, 2013].

The objective of this study is to determine the influence of tropical tropopause layer (TTL) temperature on tropical cyclone potential intensity from observations in each ocean basin separately. We will focus on the differences in TTL temperature trends as well as interannual variability between ocean basins and calculate the relative contribution, if any, of TTL temperature to changes in tropical cyclone potential intensity. We also note the signature of episodic perturbations in TTL temperatures (such as those caused by large volcanic eruptions) in tropical cyclone outflow temperature and thermodynamic efficiency.

2. Data and Methods

The potential intensity of tropical cyclones, V_p , [e.g., *Bister and Emanuel*, 1998] is defined as

$$V_p^2 = \frac{C_k}{C_D} \frac{T_s - T_o}{T_o} (h_o^* - h^*), \quad (1)$$

where C_k is the surface enthalpy exchange coefficient, C_D is the drag coefficient, T_s is the sea surface temperature, T_o is the outflow temperature, h_o^* is the saturation moist static energy of the sea surface, and h^* is the saturation moist static energy of the free troposphere. The outflow temperature is the air temperature at the level of neutral buoyancy of a parcel lifted from saturation at the sea surface temperature. Lower outflow temperatures are associated with greater thermodynamic efficiency, so it is through the efficiency term, $\frac{T_s - T_o}{T_o}$, that variations in TTL temperature may affect potential intensity. Variations in sea surface temperature primarily affect potential intensity through the disequilibrium term, $h_o^* - h^*$. The potential intensity is calculated according to the algorithm of *Bister and Emanuel* [2002]. We discuss sensitivity to the details of the potential intensity calculation in the supporting information.

We examine the contribution of the thermodynamic disequilibrium and outflow temperature to trends in potential intensity by taking the logarithm of equation (1):

$$2 \log(V_p) = \log \frac{C_k}{C_D} + \log \frac{T_s - T_o}{T_o} + \log (h_o^* - h^*). \quad (2)$$

Following *Emanuel et al.* [2013], we calculate the contribution to the decadal trend in potential intensity from each term in equation (2), for potential intensity calculated from both reanalyses and radiosonde data. C_k/C_D is taken to be a constant, 0.9, so it does not contribute to the trend in potential intensity. The efficiency term, $\log \frac{T_s - T_o}{T_o}$, is calculated directly from the sea surface temperature used in the potential intensity calculation and the resulting outflow temperature, whereas the thermodynamic disequilibrium term, $\log (h_o^* - h^*)$, is calculated as a residual from the rest of equation (2). We note that trends in this residual are not necessarily entirely due to trends in the disequilibrium term because equation (2) is an approximation to the algorithm used to calculate V_p ; we compare our results to those using a direct calculation of the disequilibrium term in the supporting information. We average each term over the peak months of the tropical cyclone season for each basin (Table 1). For the calculation from reanalyses, we perform a cosine-latitude weighted average over the regions indicated in Table 1, excluding land areas. The contribution to the decadal trend in potential intensity ($\text{m s}^{-1} \text{decade}^{-1}$) from the last two terms in equation (2) is determined by calculating the least squares regression slope of each.

Since we are analyzing trends, it is important to use radiosonde data that have been corrected for temporal inhomogeneity problems (i.e., due to instrumental changes). Two such data sets are RATPAC (radiosonde atmospheric temperature products for assessing climate) [*Free et al.*, 2005] and RATPAC-lite [*Randel and Wu*, 2006]. The main results are presented using RATPAC data, over the period 1980–2013. We also compare the results obtained from RATPAC and RATPAC-lite in the 1980–2007 period to test for sensitivity to the details of the radiosonde data (in the supporting information).

Table 1. Tropical Cyclone Main Development Regions^a

Basin	Region	Months
North Atlantic	6–18°N, 20–60°W	August–October
Eastern North Pacific	5–16°N, 90–170°W	July–September
Western North Pacific	5–15°N, 130–180°E	July–November
North Indian	5–20°N, 50–110°E,	April–November
Southern Hemisphere	5–18°S, 60–180°E	January–May

^aLatitude/longitude bounds of each tropical cyclone main development region and the peak months of the tropical cyclone season in each basin.

We select stations from the RATPAC database that are within or near the tropical cyclone basins. It is expected that the free tropospheric temperatures measured by radiosondes are representative of the basin-averaged temperatures, due to the large deformation radius in the tropics. The closest stations to the North Atlantic and eastern North Pacific main development regions are San Juan, Puerto Rico, at 18.43°N, 66°W, and Hilo, Hawaii, at 19.72°N, 155.07°W, respectively. There are three RATPAC stations located within the western North Pacific region: Koror, Palau, at 7.33°N, 134.48°E; Chuuk, Micronesia, at 7.47°N, 151.85°E; and Majuro Atoll, 7.08°N, 171.38°E. Darwin, Australia, at 12.43°S, 130.87°E, is within the Southern Hemisphere region. Bangkok, Thailand, at 13.73°N, 100.57°E, is within the North Indian region, but there is too much missing data to obtain meaningful results. For the purposes of comparing RATPAC with RATPAC-lite, we also include Marcus Island/Minamitorishima at 24.3°N, 153.97°E, which is the nearest RATPAC-lite station to the western North Pacific main development region.

Basin-averaged (Table 1) monthly mean sea surface temperatures (Hadley Centre Global Sea Ice and Sea Surface Temperature (HadISST)) [Rayner *et al.*, 2003] are used in the calculation of potential intensity from the RATPAC data. A monthly temperature climatology from the unadjusted IGRA (Integrated Global Radiosonde Archive) [Durre *et al.*, 2006] data is added to the RATPAC temperature anomalies. The potential intensity calculation also uses a monthly climatology of surface pressure and humidity from IGRA.

We also use the Interim European Centre for Medium-Range Weather Forecasts Re-Analysis (ERA-Interim) [Dee *et al.*, 2011] and the Modern-Era Retrospective Analysis for Research and Applications (MERRA) [Rienecker *et al.*, 2011]. The data used are on a monthly grid of 0.75° × 0.75° in ERA-Interim and 0.67° × 0.5° in MERRA. The work of Kossin [2014] corroborated trends in storm local upper level temperatures in the ERA-Interim and MERRA reanalyses by comparing them to tropical cyclone cloud top temperatures, giving confidence that these reanalyses are appropriate for use in this study. We do not show results using the NCEP/NCAR reanalysis [Kalnay *et al.*, 1996] because its TTL temperature trends are excessively large compared to other reanalyses and observations [Randel *et al.*, 2009; Emanuel *et al.*, 2013; Vecchi *et al.*, 2013; Kossin, 2014]. For all our results, statistical significance is assessed at the 95% confidence level, using the method described in the supporting information (which includes accounting for temporal autocorrelation in the time series).

3. Tropical Tropopause Layer Temperature

We first examine observations of temperature trends and variability in the tropical tropopause layer, in both RATPAC soundings and the ERA-Interim and MERRA reanalyses between 1980 and 2013. Figure 1 shows time series of 100 and 70 hPa temperature in the North Atlantic and western North Pacific basins as an example of how the trends and variability in TTL temperatures vary from basin to basin. In the North Atlantic, there are significant cooling trends at 70 hPa (Figure 1a) in all three data sets, although the trend in the MERRA reanalysis is significant only at the 93% confidence level. Notably, the trend in the San Juan sounding is approximately twice as large as in the reanalyses. At 100 hPa, the temperature decline is significant only in the San Juan sounding (Figure 1c). Both reanalyses and the San Juan sounding show large peaks in the 100 hPa and 70 hPa temperatures that coincide with the El Chichon and Pinatubo volcanic eruptions in 1982 and 1991, respectively. The existence of these large positive anomalies in 100 hPa and 70 hPa temperatures at the beginning of the record contributes to the overall decadal cooling trend and also supports the view that the radiative effects of large volcanic eruptions contribute to the interannual variability of temperatures in the tropical tropopause layer and lower stratosphere [Evan, 2012].

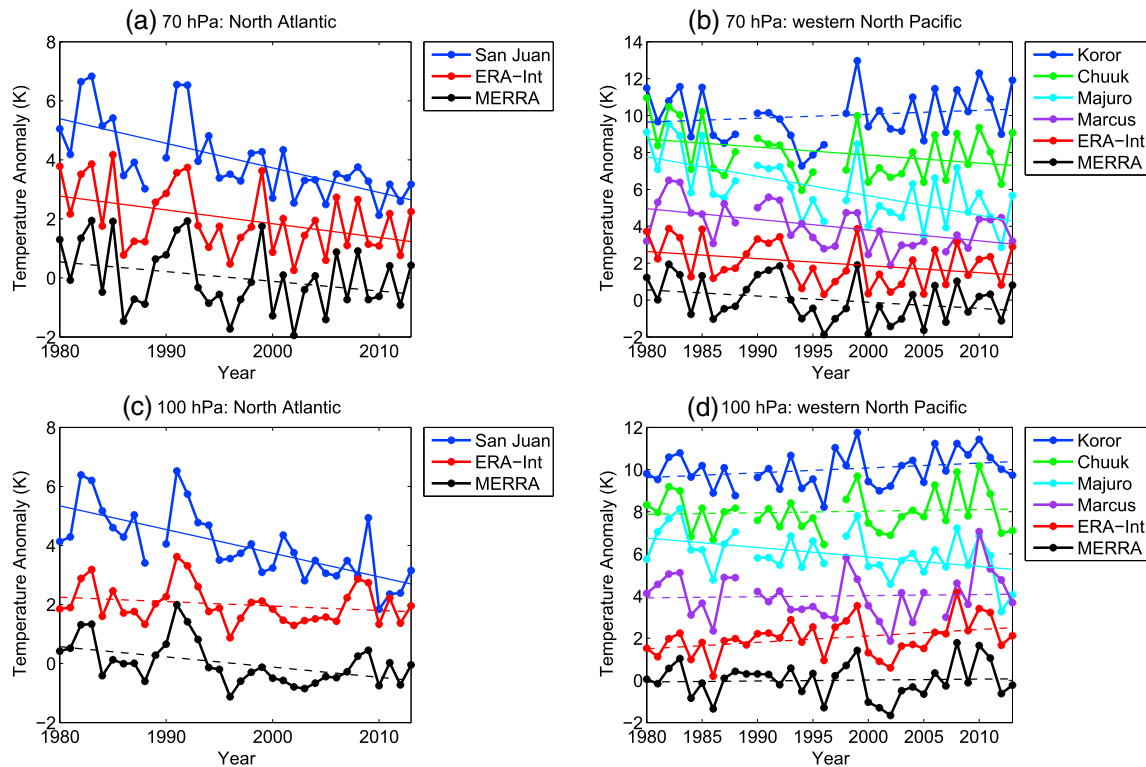


Figure 1. Temperature anomaly at 70 hPa in the (a) North Atlantic and (b) western North Pacific, averaged over the months and regions indicated in Table 1. Temperature anomaly at 100 hPa in the (c) North Atlantic and (d) western North Pacific, averaged over the months and regions indicated in Table 1. Anomalies at individual stations are from RATPAC; anomalies from reanalysis are taken from the 1980–2013 mean. Thin solid and dashed lines show the linear regression slopes; solid lines indicate that the trend is statistically significant at the 95% level. For clarity 2 K has been added successively to each time series.

In the western North Pacific at 70 hPa (Figure 1b), ERA-Interim, the Chuuk sounding, the Majuro sounding, and the Marcus Island sounding have cooling trends that are significant at the 95% confidence level (MERRA has a cooling trend that is significant at the 92% level). At 100 hPa (Figure 1d), Majuro has a statistically significant cooling trend at the 95% level, while ERA-Interim has a trend of opposite sign (but only significant at the 92% level). We note that the cold point tropopause may be above 100 hPa in the western North Pacific, and thus, these may be trends in tropospheric, not TTL, temperatures. Unlike in the North Atlantic, there is only a weak signal in 100 and 70 hPa temperatures around the time of El Chichon and no obvious signal at the time of Pinatubo. Determining the reason for this zonal asymmetry in the signal of these large volcanic eruptions is beyond the scope of this study, but possibilities include larger natural variability in the Pacific, the coincidence of an El Niño–Southern Oscillation event with the Pinatubo eruption, vertical migration of the TTL across 100 hPa, and a reduction in the relative influence of radiative effects at these levels due to stronger upward motion in the tropical western North Pacific.

In the eastern North Pacific (Figures S1a and S1b in the supporting information), ERA-Interim and the Hilo sounding have statistically significant cooling trends at 70 hPa, but at 100 hPa they disagree on the sign of the trend (only the trend in the Hilo sounding is significant at 100 hPa). There is a small peak in 70 hPa temperature that coincides with the El Chichon eruption but no obvious signal at the time of Pinatubo. In the North Indian Ocean (Figures S1c and S1d), the reanalyses have small cooling trends at 70 hPa and no trends at 100 hPa, and it is difficult to discern signals associated with El Chichon and Pinatubo, with the exception of 70 hPa temperatures at the time of El Chichon. In the Southern Hemisphere (Figures S1e and S1f), the only significant trends are a cooling trend in ERA-Interim at 70 hPa and a cooling trend in the Darwin sounding at 100 hPa (which may be below the tropopause). There are peaks in temperatures at both 70 hPa and 100 hPa in the years following the eruptions of El Chichon and Pinatubo.

Table 2. Contribution to Decadal Trend in Potential Intensity ($m s^{-1} decade^{-1}$)^a

Basin	Contribution From Disequilibrium Trend	Contribution From Efficiency Trend	Total Trend	Efficiency as Percent of Total
<i>North Atlantic</i>				
ERA-Interim	1.04	0.08	1.12	7%
MERRA	0.41	0.23	0.64	36%
San Juan	1.47	0.62	2.10	30%
<i>Eastern North Pacific</i>				
ERA-Interim	-0.11	-0.14	-0.25	57%
MERRA	-1.13	-0.04	-1.17	3%
Hilo	-0.27	0.06	-0.21	-31%
<i>Western North Pacific</i>				
ERA-Interim	0.77	-0.05	0.72	-6%
MERRA	-0.37	0.01	-0.35	-4%
Koror	0.61	-0.08	0.53	-16%
Chuuk	0.58	-0.01	0.57	-2%
Majuro	0.26	0.24	0.50	48%
Marcus	0.97	0.00	0.98	0%
<i>North Indian</i>				
ERA-Interim	0.30	0.00	0.30	0%
MERRA	-1.02	0.08	-0.94	-9%
<i>Southern Hemisphere</i>				
ERA-Interim	1.07	0.00	1.07	0%
MERRA	0.05	0.11	0.17	69%
Darwin	-0.26	0.25	-0.01	-1727%

^aContributions from the last two terms in equation (2), for the ERA-Interim and MERRA reanalyses, and RATPAC station data averaged over the months and regions defined in Table 1. Trends that are significant at the 95% confidence level are in bold font, and negative percentages indicate that the efficiency trend and total potential intensity trend are of opposite sign.

4. Decomposition of Trends in Potential Intensity

In order to determine how the trends in TTL temperature identified in the previous section translate to trends in quantities relevant to tropical cyclone intensity, we calculate the outflow temperature and potential intensity as described in section 2. As expected based on the results of the previous section, trends in tropical cyclone outflow temperature and its contribution to potential intensity vary across basin and data set. The results from a decomposition of linear trends in potential intensity from 1980 to 2013 into contributions from the last two terms on the right-hand side of equation (2) are shown in Table 2. There are statistically significant trends in potential intensity in each basin, although only the North Atlantic and western North Pacific have more than one data set with a significant trend.

The largest increase in potential intensity is found in the North Atlantic. Some of this increase is due to a trend in outflow temperature, as indicated by the ratio of the trend in the efficiency term to the total potential intensity trend (last column of Table 2). Emanuel *et al.* [2013] pointed out that most of the increase in thermodynamic efficiency, $\log \frac{T_s - T_o}{T_o}$, comes from the decrease in outflow temperature, rather than the increase in surface temperature. Since the outflow temperature is approximately the tropopause temperature, in the MERRA reanalysis and the San Juan sounding, TTL cooling contributes 30–36% of the increase in potential intensity. This result is broadly consistent with Emanuel *et al.* [2013], although they found a larger contribution of the outflow trend (40% of the total) in the San Juan sounding than found here, due to differences in how potential intensity was calculated. Kossin [2014] also found consistent outflow temperature cooling in the North Atlantic, derived from the MERRA and ERA-Interim reanalyses and tropical cyclone cloud top temperatures, although his were storm local calculations, not basin averaged. A time series of the logarithm of the

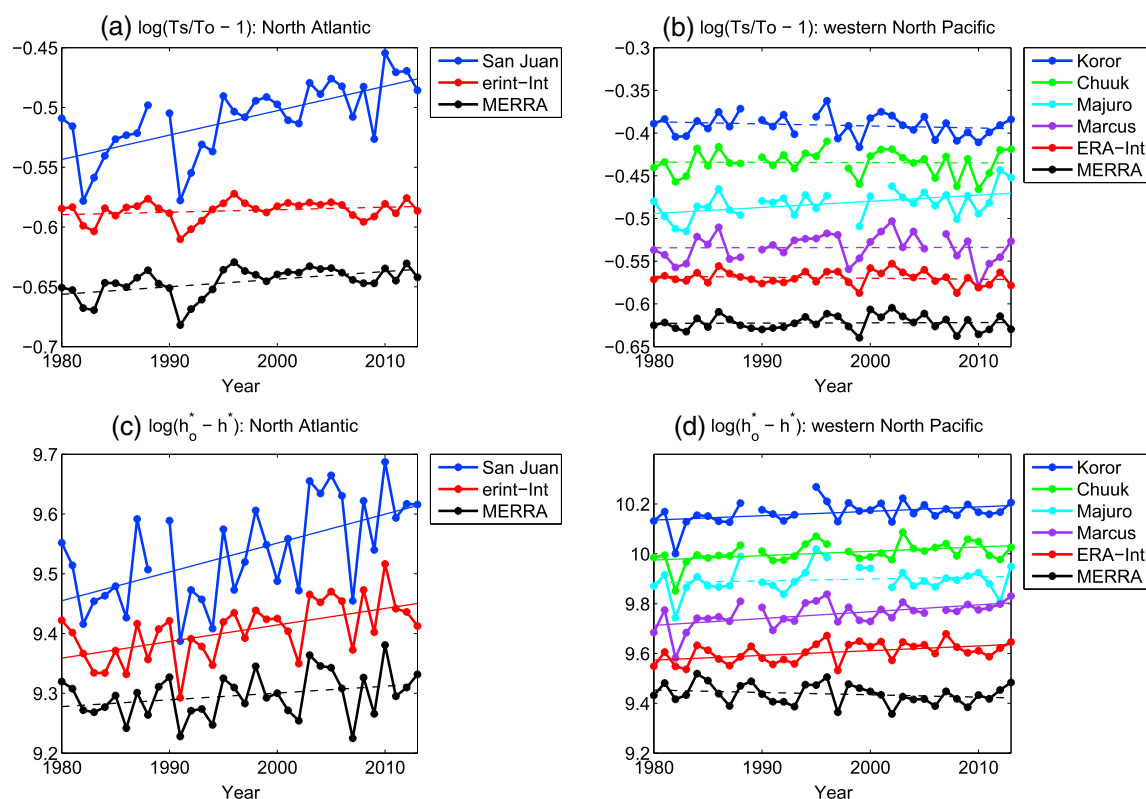


Figure 2. As in Figure 1 but for the logarithm of thermodynamic efficiency ((a, b) $\log \frac{T_s - T_e}{T_o}$) and the logarithm of thermodynamic disequilibrium ((c, d) $\log (h_o^* - h^*)$) contributions to potential intensity. The curves are offset for clarity: in Figure 2a, 0.05 is added to ERA-Interim (red) and 0.16 is added to San Juan (blue); in Figure 2b, 0.05 has been added successively to each time series; in Figure 2c, 0.05 is added to ERA-Interim (red) and 0.55 is added to San Juan (blue); in Figure 2d, 0.1 is added to ERA-Interim (red), 0.7 to Majuro (cyan), 0.8 to Chuuk (green), and 0.9 to Koror (blue).

efficiency contribution to potential intensity is shown in Figure 2a. The remainder of the increase in potential intensity is due to an increase in the thermodynamic disequilibrium (Figure 2c).

In the eastern North Pacific, the MERRA reanalysis is the only data set with a statistically significant trend in potential intensity over the last three decades, a decrease that is mostly due to a decrease in thermodynamic disequilibrium (Table 2 and Figures S2a and S2b, in the supporting information).

In the western North Pacific, there is a modest increase in potential intensity, but only the ERA-Interim and Marcus Island trends are significant at the 95% level, while trends at Koror and Chuuk are significant at 93%. In each case, the V_p increase is due to an increase in the disequilibrium term (Table 2). The increases in thermodynamic disequilibrium are also shown in Figure 2d. The Majuro sounding is an outlier and suggests that TTL cooling contributes a significant fraction (48%) of the increase in potential intensity. As shown in Figure 2b, Majuro is the only data set in which the efficiency term has a statistically significant trend. Overall, the results in the western North Pacific not only suggest a stronger role for air-sea disequilibrium than outflow temperature in potential intensity trends but also highlight the uncertainty in this result.

The results for the North Indian Ocean suggest that the contribution from thermodynamic disequilibrium dominates the potential intensity trend (Table 2). However, there is uncertainty in this result because only the MERRA reanalysis has a significant trend and the nearest RATPAC station, Bangkok, has too much missing data to corroborate it (Figures S2c and S2d).

Finally, in the Southern Hemisphere the results are inconclusive (Figures S2e and S2f). The potential intensity calculated from ERA-Interim increases significantly, entirely due to an increase in the thermodynamic disequilibrium (Table 2). The MERRA reanalysis, however, indicates an increase in the efficiency term (significant at the 90% level) that contributes a majority (69%) of the (not statistically significant) potential intensity trend. In the Darwin sounding, the trend in the disequilibrium term largely cancels the trend in the efficiency term, and only the linear trend in efficiency is statistically significant.

When the disequilibrium term is calculated directly rather than estimated as a residual, there is even less consistency in the results and it is only in the North Atlantic that we can come to a robust conclusion. As discussed in the supporting information, our results can also be sensitive to the choice of radiosonde data set and assumptions used to compute potential intensity. Overall, we find that the North Atlantic is the only basin for which there is evidence of a contribution of TTL cooling to trends in potential intensity, where it contributes up to $\sim 1/3$ of the total trend. Elsewhere, there is disagreement between the available data sets and only some of the trends are statistically significant. Most of the trends in basin-averaged potential intensity that are significant are due to trends in thermodynamic disequilibrium.

5. Interannual Variability

While trends in TTL temperatures contribute significantly to trends in potential intensity only in the North Atlantic, interannual variability in TTL temperatures could play a role in interannual variability in potential intensity, particularly variability due to large episodic perturbations such as volcanic eruptions. Figure 2a shows substantial perturbations in the thermodynamic efficiency in the North Atlantic that are coincident with the eruptions of El Chichon and Pinatubo. This is consistent with the increases in TTL temperature following those volcanic eruptions (Figures 1a and 1c). The RATPAC soundings in the western North Pacific indicate a dip in the thermodynamic efficiency at the time of the El Chichon eruption, but a signal near the Pinatubo eruption is not as apparent. The thermodynamic efficiency calculated from the ERA-Interim and MERRA reanalyses in the North Indian Ocean also contains a signal of the Pinatubo eruption (not shown). Other types of TTL temperature variability, including purely random variability, could also be important in the overall interannual variability of potential intensity.

As a simple first step to investigate the role of TTL temperature variability in potential intensity variability, we calculate the correlation between the detrended time series of seasonally averaged thermodynamic efficiency and potential intensity for each basin (the second term on the right-hand side and the first term of the left-hand side of equation (2), respectively). The time series are detrended by subtracting the linear regression line from the data. In the North Atlantic, there are statistically significant (at the 95% confidence level) correlations of $r = 0.55$, $r = 0.64$, and $r = 0.84$ in ERA-Interim, MERRA, and the San Juan RATPAC sounding, respectively. In the eastern North Pacific, there are statistically significant correlation coefficients of 0.66, 0.76, and 0.79 in ERA-Interim, MERRA, and the Hilo sounding, respectively. There is less agreement in the western North Pacific, where neither of the reanalyses has statistically significant correlations, in contrast with significant correlation coefficients of 0.68, 0.60, and 0.54 from the Koror, Chuuk, and Marcus Island soundings, respectively. In the North Indian Ocean, only data from the MERRA reanalysis has a statistically significant correlation ($r = 0.45$) between the detrended efficiency and potential intensity time series. In the Southern Hemisphere, a correlation is found only in the reanalysis data sets; $r = 0.57$ in ERA-Interim and $r = 0.64$ in MERRA. The correlation coefficients and p values for all basins and data sets are shown in Table S3.

Overall, across all basins, variance in the thermodynamic efficiency explains 20–71% of interannual variance in the potential intensity (28–71% if the North Indian basin is excluded, where only MERRA yields a correlation). Most of the interannual variance in thermodynamic efficiency is due to variance in the outflow temperature (91–99% in the Atlantic, eastern North Pacific, western North Pacific, and Southern Hemisphere basins, and 58–69% in the North Indian). Therefore, these results suggest that interannual variability in outflow temperatures, which are related to TTL temperatures, make significant contributions to interannual variability in tropical cyclone potential intensity.

6. Summary

We have demonstrated that trends in basin-averaged tropical cyclone outflow temperature and its contribution to trends in potential intensity vary between ocean basin and data set. The only robustly detectable trends are in the North Atlantic basin, where 30–36% of the positive trend in potential intensity is contributed by trends in the thermodynamic efficiency driven by TTL cooling. Trends in outflow temperature are at least partly due to warm TTL temperatures from large volcanic eruptions at the beginning of the period. Elsewhere, it is difficult to estimate potential intensity trends and their components, given the disparity in results from different data sources. However, where there are significant trends in potential intensity, they are primarily explained by trends in air-sea thermodynamic disequilibrium. This is notable because increases in sea surface temperatures, a signature of global warming [Rhein *et al.*, 2013], largely contribute to the potential intensity

through the disequilibrium term [Emanuel *et al.*, 2013]. The lack of consistent results between data sets underscores the danger of relying on a single data set for this type of analysis and reflects the uncertainties in TTL temperature trends and the limitations of reanalysis and radiosonde data.

An important new finding of this work is evidence that TTL temperatures play a significant role in the interannual variability in potential intensity over most of the world. We found statistically significant correlations between detrended time series of basin-averaged thermodynamic efficiency and potential intensity in all basins, which appear to account for 20–71 % of the variance based on a range of data sets. The interannual data are not as susceptible to the bias errors or instrument changes that are key for trends [e.g., Randel *et al.*, 2000], strengthening this conclusion. Most of the variability in thermodynamic efficiency results from variations in the outflow temperature. These results suggest that the relationship between TTL temperature variability and tropical cyclone activity warrants further study.

Understanding the contributions to trends and variability in potential intensity is an important first step, but there remains a question regarding the extent to which these results apply to changes in *actual* tropical cyclone intensity. For example, Kossin and Camargo [2009] and Kossin [2014] noted a lack of trends in global potential intensity sampled by actual tropical cyclone tracks. While most storms do not reach their potential intensity, there is some evidence that observed variations of maximum tropical cyclone intensity are consistent with variations in potential intensity [Emanuel, 2000; Wing *et al.*, 2007]. Investigating the contribution of tropical tropopause layer temperatures to interannual variability, rather than trends, in maximum intensity may therefore be a valuable extension of this work.

Acknowledgments

The MERRA data are disseminated by the Global Modeling and Assimilation Office (GMAO) and the GES DISC. The RATPAC data and IGRA data were obtained from NOAA's National Climatic Data Center, the ERA-Interim data were obtained from ECMWF, and the RATPAC-lite data were obtained from the SPARC ftp server at /sparc/ref_clim/randel/temp_trend/. The code to calculate potential intensity is available at ftp://texmex.mit.edu/pub/emanuel/TCMAX/. The HadISST data were obtained from the UK Met Office Hadley Centre. This work was supported by NSF grant AGS-1342810. The first author was additionally supported by an NSF AGS Postdoctoral Research Fellowship under award 1433251. The first author thanks Suzana Camargo, Lorenzo Polvani, and Daniel Gilford for useful discussions and Bill Randel for helpful conversations regarding RATPAC-lite. We also thank two anonymous reviewers for their insightful comments and suggestions.

The Editor thanks Robert Hodges and an anonymous reviewer for their assistance in evaluating this paper.

References

- Bister, M., and K. A. Emanuel (1998), Dissipative heating and hurricane intensity, *Meteorol. Atmos. Phys.*, *52*, 233–240.
- Bister, M., and K. A. Emanuel (2002), Low frequency variability of tropical cyclone potential intensity: 2. Climatology for 1982–1995, *J. Geophys. Res.*, *107*(D22), 4621, doi:10.1029/2001JD000780.
- Dee, D. P., et al. (2011), The ERA-Interim reanalysis: Configuration and performance of the data assimilation system, *Q. J. R. Meteorol. Soc.*, *137*(656), 553–597.
- Durre, I., R. S. Vose, and D. B. Wuertz (2006), Overview of the integrated global radiosonde archive, *J. Clim.*, *19*(1), 53–68, doi:10.1175/JCLI3594.1.
- Elsner, J. B., J. P. Kossin, and T. H. Jagger (2008), The increasing intensity of the strongest tropical cyclones, *Nature*, *455*(7209), 92–95.
- Emanuel, K. (2000), A statistical analysis of tropical cyclone intensity, *Mon. Weather Rev.*, *128*(4), 1139–1152.
- Emanuel, K. (2005), Increasing destructiveness of tropical cyclones over the past 30 years, *Nature*, *436*(7051), 686–688.
- Emanuel, K., and R. Rotunno (2011), Self-stratification of tropical cyclone outflow. Part I: Implications for storm structure, *J. Atmos. Sci.*, *68*(10), 2236–2249, doi:10.1175/JAS-D-10-05024.1.
- Emanuel, K., S. Solomon, D. Folini, S. Davis, and C. Cagnazzo (2013), Influence of tropical tropopause layer cooling on Atlantic hurricane activity, *J. Clim.*, *26*(7), 2288–2301, doi:10.1175/JCLI-D-12-00242.1.
- Emanuel, K. A. (1986), An air-sea interaction theory for tropical cyclones. Part I: Steady-state maintenance, *J. Atmos. Sci.*, *43*(6), 585–605.
- Evan, A. (2012), Atlantic hurricane activity following two major volcanic eruptions, *J. Geophys. Res.*, *117*, D06101, doi:10.1029/2011JD016716.
- Free, M., D. J. Seidel, J. K. Angell, J. Lanzante, I. Durre, and T. C. Peterson (2005), Radiosonde atmospheric temperature products for assessing climate (RATPAC): A new data set of large-area anomaly time series, *J. Geophys. Res.*, *110*, D22101, doi:10.1029/2005JD006169.
- Fueglistaler, S., A. E. Dessler, T. J. Dunkerton, I. Folkins, Q. Fu, and P. W. Mote (2009), The tropical tropopause layer, *Rev. Geophys.*, *47*, RG1004, doi:10.1029/2008RG000267.
- Haimberger, L., C. Tavolato, and S. Sperka (2012), Homogenization of the global radiosonde temperature dataset through combined comparison with reanalysis background series and neighboring stations, *J. Clim.*, *25*(23), 8108–8131, doi:10.1175/JCLI-D-11-00668.1.
- Kalnay, E., et al. (1996), The NCEP/NCAR 40-year reanalysis project, *Bull. Am. Meteorol. Soc.*, *77*(3), 437–471.
- Knutson, T. R., J. L. McBride, J. Chan, K. Emanuel, G. Holland, C. Landsea, I. Held, J. P. Kossin, A. K. Srivastava, and M. Sugi (2010), Tropical cyclones and climate change, *Nat. Geosci.*, *3*(3), 157–163.
- Kossin, J., and S. Camargo (2009), Hurricane track variability and secular potential intensity trends, *Clim. Change*, *97*, 329–337, doi:10.1007/s10584-009-9748-2.
- Kossin, J. P. (2014), Validating atmospheric reanalysis data using tropical cyclones as thermometers, *Bull. Am. Meteorol. Soc.*, *96*, 1089–1096, doi:10.1175/BAMS-D-14-00180.1.
- Kossin, J. P., T. L. Olander, and K. R. Knapp (2013), Trend analysis with a new global record of tropical cyclone intensity, *J. Clim.*, *26*, 9960–9976, doi:10.1175/JCLI-D-13-00262.1.
- Ramaswamy, V., et al. (2001), Stratospheric temperature trends: Observations and model simulations, *Rev. Geophys.*, *39*(1), 71–122.
- Ramaswamy, V., M. Schwarzkopf, W. J. Randel, B. D. Santer, B. J. Soden, and G. L. Stenchikov (2006), Anthropogenic and natural influences in the evolution of lower stratospheric cooling, *Science*, *311*, 1138–1141, doi:10.1126/science.1122587.
- Ramsay, H. A. (2013), The effects of imposed stratospheric cooling on the maximum intensity of tropical cyclones in axisymmetric radiative-convective equilibrium, *J. Clim.*, *26*(24), 9977–9985, doi:10.1175/JCLI-D-13-00195.1.
- Randel, W. J., and F. Wu (2006), Biases in stratospheric and tropospheric temperature trends derived from historical radiosonde data, *J. Clim.*, *19*(10), 2094–2104, doi:10.1175/JCLI3717.1.
- Randel, W. J., F. Wu, and D. J. Gaffen (2000), Interannual variability of the tropical tropopause derived from radiosonde cyclones NCEP reanalyses, *J. Geophys. Res.*, *105*(D12), 15,509–15,523.
- Randel, W. J., et al. (2009), An update of observed stratospheric temperature trends, *J. Geophys. Res.*, *114*, D02107, doi:10.1029/2008JD010421.

- Rayner, N. A., D. E. Parker, E. B. Horton, C. K. Folland, L. V. Alexander, D. P. Rowell, E. C. Kent, and A. Kaplan (2003), Global analyses of sea surface temperature, sea ice, and night marine air temperature since the late nineteenth century, *J. Geophys. Res.*, *108*(D14), 4407, doi:10.1029/2002JD002670.
- Rhein, M., et al. (2013), Observations: Ocean, in *Climate Change 2013: The Physical Science Basis. Contribution of Working Group I to the Fifth Assessment Report of the Intergovernmental Panel on Climate Change*, edited by T. F. Stocker et al., pp. 255–315, Cambridge Univ. Press, Cambridge, U. K., and New York.
- Rienecker, M. M., et al. (2011), MERRA: NASA's Modern-Era Retrospective Analysis for Research and Applications, *J. Clim.*, *24*(14), 3624–3648, doi:10.1175/JCLI-D-11-00015.1.
- Thompson, D. W. J., and S. Solomon (2009), Understanding recent stratospheric climate change, *J. Clim.*, *22*(8), 1934–1943, doi:10.1175/2008JCLI2482.1.
- Vecchi, G. A., S. Fueglistaler, I. M. Held, T. R. Knutson, and M. Zhao (2013), Impacts of atmospheric temperature trends on tropical cyclone activity, *J. Clim.*, *26*(11), 3877–3891, doi:10.1175/JCLI-D-12-00503.1.
- Wang, S., S. J. Camargo, A. H. Sobel, and L. M. Polvani (2014), Impact of the tropopause temperature on the intensity of tropical cyclones—An idealized study using a mesoscale model, *J. Atmos. Sci.*, *71*, 4333–4348, doi:10.1175/JAS-D-14-0029.1.
- Wing, A. A., A. H. Sobel, and S. J. Camargo (2007), Relationship between the potential and actual intensities of tropical cyclones on interannual time scales, *Geophys. Res. Lett.*, *34*, L08810, doi:10.1029/2006GL028581.